International Symposium
On Turbulence and Shear Flow
Phenomena (TSFP-9)
June 30 - July 3, 2015 *Melbourne, Australia*

NEAR-WALL BEHAVIOUR OF TRANSIENT FLOW IN A CHANNEL WITH DISTRIBUTED PYRAMID ROUGHNESS

Mehdi Seddighi
Department of Mechanical Engineering
University of Sheffield
Sheffield, UK, S1 3JD
seddighi@sheffield.ac.uk (Corresponding author)

Shuisheng He
Department of Mechanical Engineering
University of Sheffield
Sheffield, UK, S1 3JD
s.he@sheffield.ac.uk

Dubravka Pokrajac
School of Engineering
University of Aberdeen
Aberdeen, UK, AB24 3UE
d.pokrajac@abdn.ac.uk

Tom O′Donoghue
School of Engineering
University of Aberdeen
Aberdeen, UK, AB24 3UE
t.odonoghue@abdn.ac.uk

Alan Vardy
Division of Civil Engineering
University of Dundee
Dundee, UK, PH14 9SS
a.e.vardy@dundee.ac.uk

ABSTRACT

DNS has been performed to investigate near-wall behaviour of turbulence for a rapid 'turbulent-to-turbulent' transient flow in a channel with a smooth top surface and a rough bottom surface made of close-packed pyramids. The transient flow is studied following a rapid change in flow rate from $Re = 2800$ to $Re = 7400$. The equivalent roughness heights normalised by the wall units, k_s^+, of the initial and final flows are, respectively, 14.5 and 41. The results show that near-wall behaviour of turbulence in the early stages of the transient process for the rough wall differs significantly from that over the smooth-wall. The early transient process over the rough-wall is in the form of a single cycle of birth, evolution and eventually breakdown of strong primary counter-rotating hairpin structures in the region very close to the roughness crests. Similar to that in a steady flow, the direct effect of roughness in a transient flow is confined to a region up to approximately three times of roughness height above the crest. Though the transient process starts from an initially fully-developed turbulent flow, the early transient process exhibits a roughness-induced laminar-turbulent transition. Various statistical quantities, including the three components of r.m.s. of velocity fluctuations and also turbulent shear stress, confirm the visualisation results.

INTRODUCTION

Unsteady flows, in which the bulk velocity of a wall-bounded flow or the free-stream velocity of a boundary-layer flow vary with time, are encountered in many engineering applications. Previous studies of non-periodic transient flows over smooth-surfaces include Greenblatt & Moss (1999); He & Jackson (2000); Greenblatt & Moss (2004); Chung (2005); He *et al.* (2008, 2011); Seddighi *et al.* (2011); Jung & Chung (2012). It has been established that in a temporally-accelerating flow over smooth surfaces, the unsteady flow behaviour is largely associated with the response of turbulence. Initially, there is a short period when turbulence is effectively "frozen". This is followed by the response of turbulence, first in the streamwise component in the near-wall region. Later, the streamwise turbulent energy is redistributed into the other two components. The response of the turbulence then propagates into the core of the flow with progressively longer delays.

Recent Direct Numerical Simulation (DNS) of transient channel flow with wholly smooth wall surfaces (He & Seddighi, 2013; Seddighi *et al.*, 2014) have shown that, following a flow acceleration of an initially steady turbulent flow, turbulence exhibits a process of transition that resembles laminar-turbulent bypass transition, rather than progressively evolving from the initial turbulent structure to a new one. The detailed studies of He & Seddighi (2013) and Seddighi *et al.* (2014) for rapid and slow accelerations, respectively, have shown that the overall behaviour of the transition over a smooth wall largely depends on the initial and final flow conditions. The acceleration rate, however, may significantly alter the transition onset. The transient flow undergoes three distinct phases: (i) pre-transition, the flow is laminar-like and the pre-existing turbulent structures are modulated, resulting in elongated streaks leading to a strong and continuous increase in the streamwise fluctuating velocity, but little change in the other two components; (ii) the flow then undergoes transition with isolated turbulent spots being generated and then spreading and merging with each other; (iii) the turbulent spots eventually cover the entire surface of the wall and the flow is fully turbulent. More recently, He & Seddighi (2015) systematically varied the initial and final Reynolds numbers of the near-step transition flows. It was shown that, for all conditions, the transient flow is characterised by laminar-turbulent transition, which exhibits itself clearly in the flow statistics. This is despite the fact that when final-to-initial Reynolds number ratio is low (such as 1.1), the flow does not exhibit either elongated streaks or isolated turbulent spots, both of which are present when the final-to-initial Reynolds number ratio is high. The time developing boundary layer in the pre-transition phase follows closely the Stokes solution for a transient laminar boundary layer.

All of the above studies were for smooth-wall surfaces

and this is despite the fact that most engineering applications involve rough surfaces. Roughness has the potential to induce an enhanced laminar-turbulent transition that can significantly increase the friction factor. Aeronautical applications are important examples of external flows in which roughness can induce a laminar-turbulent transition (known as roughness-induced transition), leading to a significant influence on aerodynamic performance and heat transfer. In experimental studies with compact 3D roughness, the measurements are often necessarily limited to the region above the roughness crests (e.g. Hong *et al.* 2012). The present paper reports on a DNS study of turbulence in a transient flow in a channel with a bottom wall having distributed roughness elements with height of 0.05δ, where δ is the channel half-height.

METHODOLOGY

The DNS is performed using an in-house code (Seddighi, 2011; He & Seddighi, 2013). The governing equations are written in dimensionless form, normalised using δ for length, U_c(centreline laminar Poiseuille velocity) for velocity, and ρU_c^2 for pressure:

$$\frac{\partial u_i^*}{\partial t^*} + u_j^* \frac{\partial u_i^*}{\partial x_j^*} = -\frac{\partial p^*}{\partial x_i^*} + \frac{1}{Re_c}\frac{\partial^2 u_i^*}{\partial x_j^* \partial x_j^*} + \Pi \qquad (1)$$

$$\frac{\partial u_i^*}{\partial x_i^*} = 0 \qquad (2)$$

The Reynolds number is defined as $Re_c = \frac{\delta U_c}{\nu}$. However, for ease of explanation of the results, unless otherwise stated, the time presented in this paper is rescaled using the bulk velocity of the initial flow (U_{b0}) as the characteristic velocity. The pressure gradient is split into two components, namely Π and $\frac{\partial p^*}{\partial x_i^*}$. The former is the spatially-uniform, time-mean component of the streamwise pressure gradient required to balance the resistance due to friction and form drag (i.e. the value that would be needed to maintain a constant mass flow rate). In an unsteady flow it also provides an additional force to maintain the acceleration. The $\frac{\partial p^*}{\partial x_i^*}$ component is a fluctuating component that varies both spatially and with time due to turbulence and flow heterogeneity.

A second order finite difference method is used to discretise the spatial derivatives of the governing equations on a rectangular grid. An explicit 3rd order Runge-Kutta scheme and an implicit second order Crank-Nicholson scheme are incorporated into the fractional-step method (Orlandi, 2001). The Poisson equation for the pressure is solved by an efficient 2-D FFT. The equations are solved in a domain of 9.6δ, 2δ, 4.5δ, with a mesh of $1024 \times 240 \times 720$ in the streamwise (x), wall-normal (y), and spanwise (z) directions, respectively. The roughness is treated using a revised version of an immersed boundary technique described by Fadlun *et al.* (2000). The Message-Passing Interface (MPI) is used to parallelize the code, which has been extensively validated for steady channel flow results against commonly-used databases.

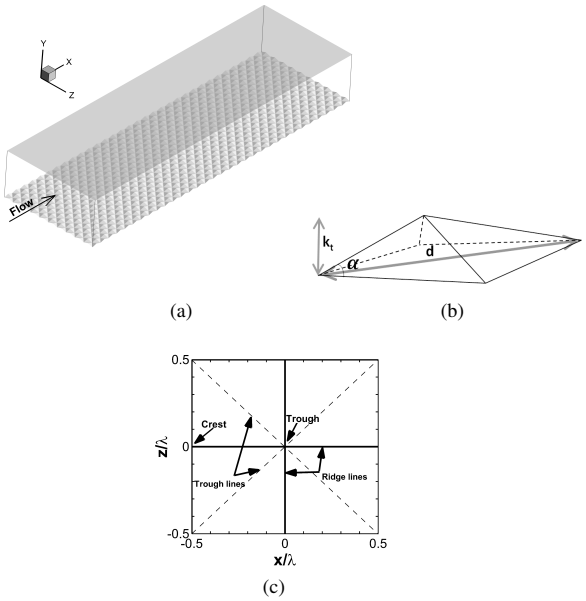

Figure 1: (*a*) Rough-wall roughness structure; (*b*) Geometric parameters for roughness pyramid: $k_t = 0.05(\delta)$, $\lambda = d = 0.3(\delta)$, $\alpha \approx 18.4^\circ$; (*c*) x-z plane view of one wavelength of roughness.

RESULTS AND DISCUSSION

The channel has a smooth top surface and a close-packed pyramid-roughened bottom surface (Figure 1). The slope angle of the lateral edge of the pyramid with the horizontal plane is $\alpha \approx 18.4^\circ$ and the height of the roughness is $\frac{k_t}{\delta} = 0.05$, where k_t is the peak-to-trough roughness height. The flow is initially steady and is in the transitionally rough regime; the flow rate is then rapidly increased to a much higher level, leading to near fully-rough flow once steady conditions are reached. The initial and final Reynolds numbers of the transient flow are $Re_0 = 2800$ and $Re_1 = 7400$ respectively, where $Re = \frac{\delta U_b}{\nu}$, with U_b the bulk velocity and ν the fluid kinematic viscosity. The corresponding equivalent heights (k_s^+) are approximately 14.5 and 41, respectively.

Figure 2 shows three-dimensional iso-surface plots of negative pressure and λ_2 at several instants of the transient flow. For clarity, only $1/4$ of the streamwise and $1/5$ of the spanwise extent of the simulated domain is shown. The time (t*) is normalised by δ and U_b. Here, λ_2 is the second largest eigenvalue of the symmetric tensor $S^2 + \Omega^2$ where S and Ω are the symmetric and antisymmetric parts of the velocity gradient tensor, Δu. The negative iso-surface of λ_2 is used to identify vortex cores (Jeong & Hussain, 1995). All visualised quantities are normalized by wall units of the initial flow. Soon after the commencement of the transient (t*=0.09), a region of strong vortex (shown by λ_2 iso-surface) develops around the roughness crest, extending along the spanwise ridge line. Later, a well-organised, roughness-induced, strong, head-up hairpin structure is generated around each roughness element. These vortices, which are similar to each other in both size and strength over all elements in the flow domain, then convect downstream and subsequently evolve. Later (t*=0.2), the vortex is split into two parts. One part remains at the location of its birth (that is at the crest of the roughness element) throughout the rest of the transient process (see later instants). The second part is convected downstream

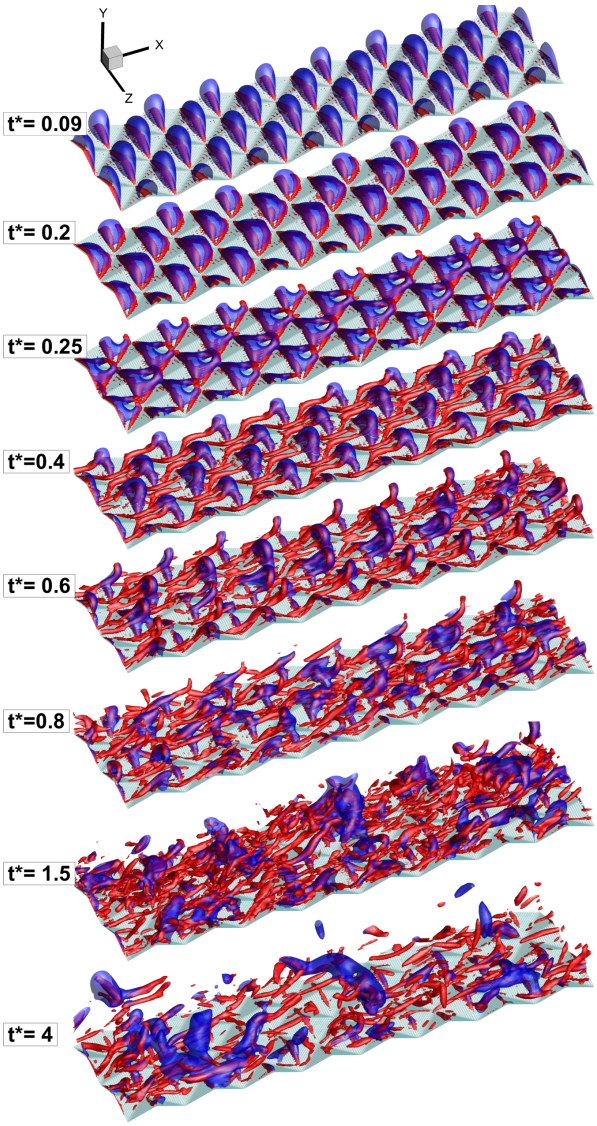

Figure 2: Flow structures in iso-surface plots; 3-D plots of pressure and λ_2, coloured by blue ($p/\rho u_{\tau 0}^2 = -1.2$) and red ($\frac{\lambda_2}{(u_{\tau 0}/\delta)^2} = -1.1$), respectively; for clarity, data are shown for part of the computational domain (1/4 and 1/5 in streamwise and spanwise directions, respectively).

and plays a major role in the transition. The lower parts of this new vortex traverse alongside the two trough lines, and the upper necklace part located behind the roughness crest goes downstream along the ridge line. At t*=0.25, a typical primary hairpin vortex has emerged, with two counter rotating legs alongside the ridge lines and the head in the roughness wake (around the trough). This vortex has travelled half of the roughness wavelength ($x/\lambda = 0.5$, where λ is the roughness wavelength) by this instant. At this stage, the vortices are still very close to the surface. By t*$\sim$0.4, the head of the quasi-streamwise primary vortex has reached the crest of the successive roughness element, and starts to move away from the wall. It is also seen that the region of

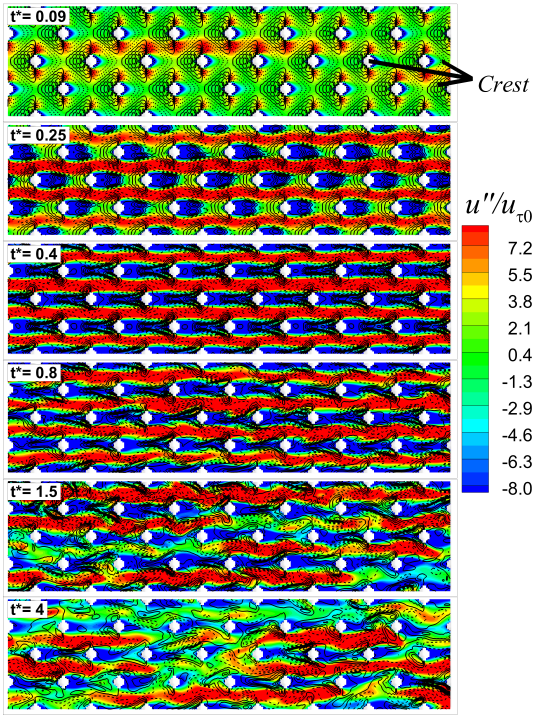

Figure 3: Streamwise fluctuating velocity (contour shaded) and wall-normal velocity (contour line) for a plane at $y = -0.2k_t$ below the crest of the roughness element, at several instants during the transient flow; only part of the computational domain is shown; negative wall-normal velocity values are represented by dashed lines.

the strong hairpin vortices is associated with the low pressure region (shown by blue structures). From about t*=0.8, a significant burst of the primary hairpins is observed and the vortices are replaced by more random and smaller vortical structures. By t*$\sim$4, there are no strong structures identified near the roughness and the flow in the roughness sublayer has effectively reached the final flow condition.

The existence of standing and hairpin vortices, and the evolution and breakdown of the latter in the transient flow bears a strong qualitative resemblance to those of the roughness-induced laminar-turbulent transition described by Acarlar & Smith (1987) for low-speed Blasius boundary layer and De Tullio *et al.* (2013) for supersonic boundary layer for an isolated roughness element. This is particularly interesting considering that in the present case i) the initial flow is a turbulent flow in the transitionally rough regime ($k_s^+ \sim$15); and ii) the transient process occurs over the surface which is entirely covered by close-packed distributed roughness elements in both the streamwise and spanwise directions.

Figure 3 shows the development of streamwise fluctuating and normal velocities for a plane at $y = -0.2k_t$ below the crest of the roughness element. Here the streamwise fluctuating velocity is $u" = u - \langle\overline{u}\rangle$, where u is the instantaneous streamwise velocity and $\langle\overline{u}\rangle$ is the velocity averaged spatially (in both streamwise and spanwise directions) as well as over the number of repeated runs. It is seen that at the very early stage of the transient flow (t*=0.09),

the forward side of the element is the locus of the positive wall-normal velocity, whereas the lee-side is the region with the negative values. At t*=0.25, strong positive streamwise velocity fluctuations are seen along the troughs of the roughness elements, forming high-speed streaks in these regions. At this time, patches of strong negative velocity are also formed within the primary vortices. At a later time (t*=0.4), such patches are connected, forming negative velocity streaks. This instant corresponds to the time when the heads of the primary vortices move away from the wall (see figure 2). This creates a situation where all the primary vortices sit on top of the negative streaks, which is a typical scenario identified in bypass transition (Jacobs & Durbin, 2001). In fact the positive and negative streaks are themselves supporting evidence of the existence of a strong counter-rotating vortex (Alfonsi, 2006). At t*=0.8, the elongated negative and positive streaks have become more wavy-like structures, and start to break up. At later instants the well-organised elongated streaks have disappeared.

Figure 4 shows the development of the friction coefficient for the transient flow. Also shown are the results of He & Seddighi (2013) for a channel with smooth top and bottom walls ('smooth-case'). It is seen that the development of the friction coefficient for the smooth wall is consistent with the results of (He & Seddighi, 2013), exhibiting a bypass transition behaviour. A large undershoot, until t*∼8, exhibited by the smooth wall is characteristic of the flow in the pre-transition stage during which the flow exhibits a trend of a laminar friction factor (He & Seddighi, 2015). The friction factor for the rough wall, however, shows a trend that is significantly different from that of the smooth wall. The development shows neither a large undershoot in the initial stages, nor a long delay (t*∼16) before reaching the corresponding final flow value. This behaviour is not a surprise noting that strong hairpin vortices are generated very early in time (t*∼0.25), and the transition is completed by t*∼4. The variation of C_f is largely dominated by the relaxation of the mean velocity profile which causes a continual reduction from its initial peak value resulting from the sudden increase in flow rate. The effect of the primary vortex generated at t*∼0.25 is reflected as a kink in the variation of C_f (see the inset). In the period of $0.25 < t^* < 0.8$, the profile shows an oscillatory variation with several further kinks. The period corresponds to the time during which the primary vortices are pumping up from the wall, whilst convecting downstream the flow. The vortices remain in $\frac{y}{k_t} < 1$ until the transition time (t*∼0.8), when the major breakup of the primary vortices has started to occur.

Figure 5 shows the development of the turbulent shear stress and r.m.s. of velocity fluctuations for the y-z plane at $x/\lambda = 0.49$ at several instants. The streamwise velocity fluctuation (and similarly for the wall-normal and spanwise components) used here is defined as $u' = u - \overline{u}$, where $\overline{u}$ is the mean velocity averaged over the repeated runs as well as the roughness elements in the streamwise and spanwise directions. The normalisation of the visualised values is based on the friction velocity for the rough wall at the initial Reynolds number. At t*=0.25 (the first column from the left), the locus of high turbulent region for all Reynolds stress components is above the trough of the roughness element. This is the signature of the legs of strong primary hairpins (see figure 2) when they form alongside the ridge lines. Later, at t*=0.4, the high-value regions occur above

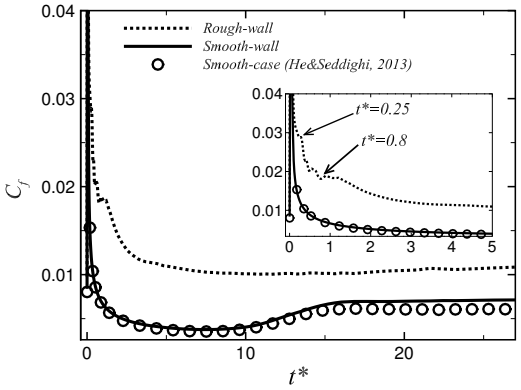

Figure 4: Development of the skin friction coefficient, C_f, for the unsteady case; symbols show the smooth wall results of He & Seddighi (2013).

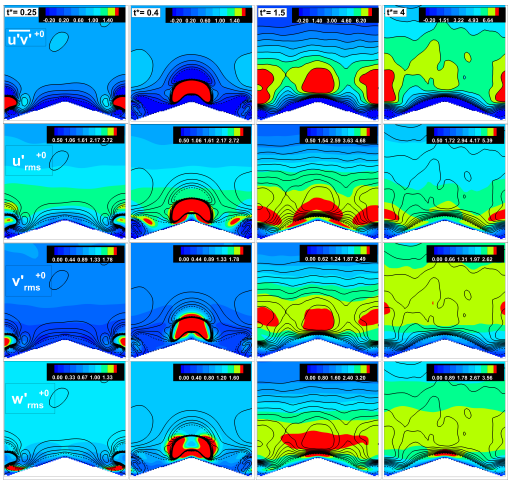

Figure 5: Turbulent shear stress and r.m.s. of velocity fluctuations during the transient flow for the y-z plane at $x/\lambda = 0.49$.

the crest of the element. This instant corresponds to the time when the primary hairpin is formed and has reached the crest of the successive element (see figure 2). This shows that, although vortices of various strengths are formed behind each roughness element, the strong primary vortices have the most striking impact on the near-wall turbulence structure in the early stages of the transient flow. It is also interesting that the distribution and values of $u'_{rms}{}^{+0}$, $v'_{rms}{}^{+0}$ and $w'_{rms}{}^{+0}$ in the near-wall region are similar, indicating that the Reynolds stress anisotropy is much reduced close to the roughness element. At t*=1.5, the break-up of the primary hairpins has already started, but the traces of these and other vortices that existed previously are shown as intense-value regions. The organised intense-patches have disappeared at t*=4 (the plots in the last-right column), which is consistent with figure 2, when the organised primary and subsequent vortices have disappeared from the near-wall region.

To examine further the influence of the roughness on the development of the turbulence structure, pre-multiplied streamwise energy spectra of the fundamental wavelength

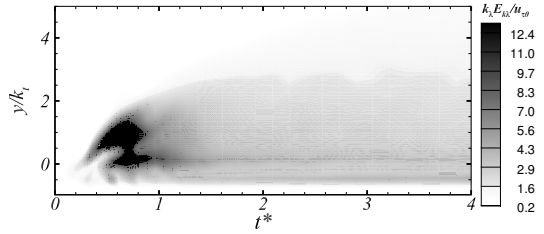

Figure 6: Development of pre-multiplied spectra of the fundamental wavelength (λ) for $\overline{\langle u'u' \rangle}$ in the streamwise direction.

are presented in Figure 6. The energy spectra of the streamwise normal stress, E_{11}, are defined such that

$$\overline{\langle u'u' \rangle} = \int_0^\infty E_{11} dk \tag{3}$$

It has been found that (not shown) the main influence of roughness on the streamwise energy spectra during the early stages of the transient flow is the presence of spikes at wavenumber of $k_\lambda = 2\pi/\lambda = 20.94$ (wavenumber corresponding to the roughness wavelength, $\lambda = 0.3$) and its multiples. Figure 6 shows development of the energy spectra associated with the fundamental wavelength $k_x = k_\lambda$ for the locations up to $\frac{y}{k_t} = 5$. An area of high energy spectra is seen for the locations up to $\frac{y}{k_t} \sim 1.5$ during $0.3 < t^* < 0.8$. This indicates that strong influence of the fundamental wavelength is restricted up to $\frac{y}{k_t} \sim 3$ and the effect lasts until t* $\sim$0.8 when the major breakdown of the primary hairpin structures starts to occur.

The transport equations for the Reynolds stresses over the smooth wall are as follows:

$$0 = -I_{ij} + C_{ij} + P_{ij} + T_{ij} + D_{ij} + \Pi_{ij_{strain}} + \Pi_{ij_{diffusion}} + \varepsilon_{ij} \tag{4}$$

The terms on the RHS are, respectively, inertia (I_{ij}), advection (C_{ij}), turbulent production (P_{ij}), turbulent transport rate (T_{ij}), viscous diffusion rate (D_{ij}), pressure velocity-gradient (strain term) ($\Pi_{ij_{strain}}$), pressure velocity-gradient (diffusion term) ($\Pi_{ij_{diffusion}}$) and turbulence dissipation rate (ε_{ij}). For turbulent-only quantities, I_{ij}, P_{ij}, $\Pi_{ij_{strain}}$ and ε_{ij} are defined as

$$I_{ij} = \frac{\partial \langle \overline{u_i' u_j'} \rangle}{\partial t}$$

$$P_{ij} = -\left(\langle \overline{u_i' u_k'} \rangle \frac{\partial \langle \overline{u_j} \rangle}{\partial x_k} + \langle \overline{u_j' u_k'} \rangle \frac{\partial \langle \overline{u_i} \rangle}{\partial x_k} \right)$$

$$\Pi_{ij_{strain}} = \langle \overline{p' \frac{\partial u_i'}{\partial x_j}} \rangle + \langle \overline{p' \frac{\partial u_j'}{\partial x_i}} \rangle$$

$$\varepsilon_{ij} = -2\nu \langle \overline{\frac{\partial u_i'}{\partial x_k} \frac{\partial u_j'}{\partial x_k}} \rangle$$

Repeated indices indicate summation over 1,2,3. Figure 7 shows profiles of the above selected budget terms for the streamwise Reynolds stress , $\frac{\overline{\langle u'u' \rangle}}{u_{\tau_0}^4/\nu}$ for several time instants. Also shown in each frame are the corresponding values of each term at a time when the flow has reached the final steady flow condition. The normalisation based on u_{τ_0} rather than u_τ enables the absolute response of the budget terms to be seen. The earliest response occurs very close to the roughness crest (the elevation relative to the roughness height is shown at the top of the graph and y'^{+0} at the bottom).

The production term is featured with several peaks which appear and develop at various times during the transient period. At t*=0, the peak production is around $y'^{+0} \approx 10$ (or $\frac{y}{k_t} \sim 0.5$) as expected from typical behaviour in steady shear flows (the peak is marked as "1" in the plot). This peak value remains more or less unchanged at t*=0.17, and at the same time a second peak (marked as "2") is formed below the crest of the roughness. This second peak increases in magnitude and moves away from the wall with time. A third peak (marked as "3") is formed around t*=0.4 around the crest of the roughness, increasing rapidly in amplitude but remaining largely unchanged in location. These various peaking productions signify different stages of turbulence development. The second peak production corresponds to the formation and development of the primary vortices. The location and timing of this peak production follow closely the formation of the primary vortices and their lift-up from the wall with time. The third peak in production corresponds to a strong shear layer formed around the roughness crest due to the increase in flow rate, and also an increased turbulent shear stress associated with the formation and movement of the vortices generated during the early times (say, up to t*=1.5). Between t*=0.6 and 1.5, the production significantly overshoots the steady values, mostly due to the strong shear layer and the presence of violent vortices during this period. After t*=0.8, the overshooting reduces, which corresponds to the time when the large vortices are ejected from the wall, break down and are replaced with turbulence structures that are commensurate with the final steady flow.

In comparison with the flow over a smooth wall, the response of the pressure-strain term occurs much earlier in the rough wall case. This is no surprise as the 3D roughness elements impose an early interaction between the pressure and velocity fields, and hence an earlier transfer of energy from $\overline{\langle u'u' \rangle}$ to $\overline{\langle v'v' \rangle}$ and $\overline{\langle w'w' \rangle}$. Another point to note is that the inertia makes a large positive contribution to the budget balance at the early times (t*=0.25 to 0.8), but is negative (with relatively smaller magnitude) at t*=1.5, indicating a reduction in $\overline{\langle u'u' \rangle}$.

CONCLUSIONS

Direct Numerical Simulation has been performed of a transient flow in a channel consisting of a rough bottom wall made of close-packed pyramid roughness and a smooth top wall. The unsteady flow started from an initially statistically steady turbulent flow with $Re = 2800$ and increased linearly, within a very short time, to a final Reynolds number of $Re = 7400$. The corresponding equivalent sand roughness Reynolds numbers for the initial and final flows are respectively k_s^+=14.5 and k_s^+=41.

The results show that near-wall behaviour of turbulence during the early stages of transient flow over the rough wall differ significantly from that over the smooth wall. The early stages of the transient process for the rough wall are

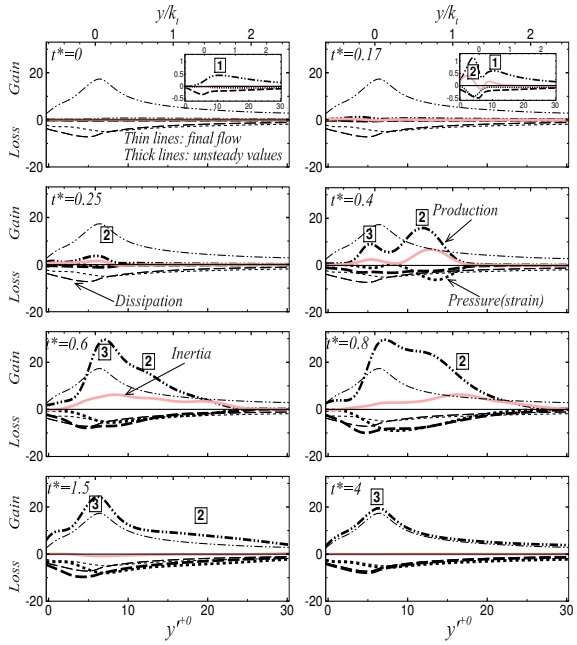

Figure 7: Development of several terms of the Reynolds stress budget $\langle \overline{u'u'} \rangle$ normalised with u_τ^4/ν, for the rough wall at several instants.

dominated by a single cycle of birth, evolution and breakdown of strong primary counter-rotating hairpin structures. Over each roughness element, a vortex is formed with its head behind the roughness crest and its legs alongside the ridge lines. Most of the strong hairpin structures lift up to the upper layers and break down before t*∼4. In addition to the generation of primary vortices, positive and negative streaks are produced and these break up at the same time as the vortices break down. Soon after (t*∼4), the flow near the wall has reached its new turbulence state and the primary process of the transition is complete. Significant further time (t*∼27.2) is needed for the new turbulence to propagate into the core of the channel flow. The vortices generated around the close-packed roughness elements resemble closely the hairpin structures formed over isolated roughness in the transition of a laminar boundary layer (Acarlar & Smith, 1987). The flow over the upper, smooth wall of the channel undergoes bypass transition that is closely similar to that reported by He & Seddighi (2013) for a wholly smooth channel. It is especially noteworthy that the much earlier transition on the opposite rough wall has no significant influence on the timing and process of the transition on the smooth wall.

REFERENCES

Acarlar, M. S. & Smith, C. R. 1987 A study of hairpin vortices in a laminar boundary layer. part 1. hairpin vortices generated by a hemisphere protuberance. *Journal of Fluid Mechanics* **175**, 1–41.

Alfonsi, G. 2006 Coherent structures of turbulence: Methods of eduction and results. *Applied Mechanics Reviews* **59** (1-6), 307–323.

Chung, Y. M. 2005 Unsteady turbulent flow with sudden pressure gradient changes. *International Journal for Numerical Methods in Fluids* **47** (8-9), 925–930.

De Tullio, N., Paredes, P., Sandham, N. D. & Theofilis, V. 2013 Laminarturbulent transition induced by a discrete roughness element in a supersonic boundary layer. *Journal of Fluid Mechanics* **735**, 613–646.

Fadlun, E. A., Verzicco, R., Orlandi, P. & Mohd-Yusof, J. 2000 Combined immersed-boundary finite-difference methods for three-dimensional complex flow simulations. *Journal of Computational Physics* **161** (1), 35–60.

Greenblatt, D. & Moss, E. A. 1999 Pipe-flow relaminarization by temporal acceleration. *Physics of Fluids* **11** (11), 3478–3481.

Greenblatt, D. & Moss, E. A. 2004 Rapid temporal acceleration of a turbulent pipe flow. *Journal of Fluid Mechanics* **514**, 65–75.

He, S., Ariyaratne, C. & Vardy, A. E. 2008 A computational study of wall friction and turbulence dynamics in accelerating pipe flows. *Computers and Fluids* **37** (6), 674–689.

He, S., Ariyaratne, C. & Vardy, A. E. 2011 Wall shear stress in accelerating turbulent pipe flow. *Journal of Fluid Mechanics* **685**, 440–460.

He, S. & Jackson, J. D. 2000 A study of turbulence under conditions of transient flow in a pipe. *Journal of Fluid Mechanics* **408**, 1–38.

He, S. & Seddighi, M. 2013 Turbulence in transient channel flow. *Journal of Fluid Mechanics* **715**, 60–102.

He, S. & Seddighi, M. 2015 Transition of transient channel flow after a change in Reynolds number. *Journal of Fluid Mechanics* **764**, 395–427.

Hong, J., Katz, J., Meneveau, C. & Schultz, M. P. 2012 Coherent structures and associated subgrid-scale energy transfer in a rough-wall turbulent channel flow. *Journal of Fluid Mechanics* pp. 1–37.

Jacobs, R. G. & Durbin, P. A. 2001 Simulations of bypass transition. *Journal of Fluid Mechanics* **428** (1), 185–212.

Jeong, J. & Hussain, F. 1995 On the identification of a vortex. *Journal of Fluid Mechanics* **285**, 69–94.

Jung, S. Y. & Chung, Y. M. 2012 Large-eddy simulation of accelerated turbulent flow in a circular pipe. *International Journal of Heat and Fluid Flow* **33** (1), 1–8.

Orlandi, P 2001 *Fluid flow phenomena: a numerical toolkit*. Kluwer.

Seddighi, M. 2011 Study of turbulence and wall shear stress in unsteady flow over smooth and rough wall surfaces. PhD thesis, University of Aberdeen.

Seddighi, M., He, S., Orlandi, P. & Vardy, A. E. 2011 A comparative study of turbulence in ramp-up and ramp-down unsteady flows. *Flow, Turbulence and Combustion* **86** (3-4), 439–454.

Seddighi, M., He, S., Vardy, A. E. & Orlandi, P. 2014 Direct numerical simulation of an accelerating channel flow. *Flow, Turbulence and Combustion* pp. 1–30.